energies

MDPI

Article

Optimizing Current Profiles for Efficient Online Estimation of Battery Equivalent Circuit Model Parameters Based on Cramer–Rao Lower Bound

Prarthana Pillai [1], Sneha Sundaresan [1], Krishna R. Pattipati [2] and Balakumar Balasingam [1,*]

[1] Department of Electrical and Computer Engineering, University of Windsor, Windsor, ON N9B 3P4, Canada
[2] Department of Electrical and Computer Engineering, University of Connecticut, Storrs, CT 06269, USA
* Correspondence: singam@uwindsor.ca; Tel.: +1-(519)-253-3000 (ext. 5431)

Abstract: Battery management systems (BMS) are important for ensuring the safety, efficiency and reliability of a battery pack. Estimating the internal equivalent circuit model (ECM) parameters of a battery, such as the internal open circuit voltage, battery resistance and relaxation parameters, is a crucial requirement in BMSs. Numerous approaches to estimating ECM parameters have been reported in the literature. However, existing approaches consider ECM identification as a joint estimation problem that estimates the state of charge together with the ECM parameters. In this paper, an approach is presented to decouple the problem into ECM identification alone. Using the proposed approach, the internal open circuit voltage and the ECM parameters can be estimated without requiring the knowledge of the state of charge of the battery. The proposed approach is applied to estimate the open circuit voltage and internal resistance of a battery.

Keywords: battery management system; battery equivalent circuit model; least squares estimation; battery internal resistance; Cramer–Rao lower bound

check for updates

Citation: Pillai, P.; Sundaresan, S.; Pattipati, K.R.; Balasingam, B Optimizing Current Profiles for Efficient Online Estimation of Battery Equivalent Circuit Model Parameters Based on Cramer–Rao Lower Bound. *Energies* **2022**, *15*, 8441. https://doi.org/10.3390/en15228441

Academic Editors: Frede Blaabjerg and Abu-Siada Ahmed

Received: 27 September 2022
Accepted: 9 November 2022
Published: 11 November 2022

1. Introduction

Rechargeable Li-ion batteries are becoming ubiquitous in wide-ranging applications, such as electric vehicles, consumer electronics, power equipment and aerospace systems [1,2]. A battery management system (BMS) is required to ensure the safe, efficient and reliable operation of battery packs. It is quite well known that Li-ion batteries suffer from safety issues when operated outside their allowable voltage ranges. It is the task of the BMS to keep the battery within the operable range to ensure safety. A battery pack that is not properly managed is neither efficient nor reliable. For example, a pack that is not balanced is limited in its performance due to weak cells. Such cells can make the pack useless over time. Consequently, the BMS constantly monitors the battery by measuring the voltage and current of the battery to perform specific control operations [3]. Using the measured data, the BMS accurately estimates crucial diagnostic parameters of a battery pack, such as battery equivalent circuit model parameters (ECM) [4,5], battery capacity [6–8], state of charge (SOC) [9], state of health (SOH) [10,11], time to shut down and the remaining useful life (RUL) [12].

Estimation of the electrical equivalent circuit model parameters of the battery is a wide area of research. The estimated ECM parameters are used to model the voltage drop within the battery, eventually to estimate the SOC by the voltage-based approach [13]. The estimated ECM parameters, along with the estimated SOC, can be used to compute the remaining mileage of an electric vehicle. ECM parameters determine the limits of charging current for safe and fast charging of batteries. In battery thermal management, with the identified ECM parameters, heat generated within the battery can be computed to predict the surface temperature of batteries [14] so that it can be maintained within safe temperature limits.

Existing approaches to the estimation of ECM parameters can be broadly divided into time domain and frequency domain approaches. Time domain approaches are methods which use instantaneous voltage and current measurements to estimate ECM parameters. In the frequency domain, battery ECM parameters are estimated through electrochemical impedance spectroscopy (EIS) [15]. EIS approach to battery ECM parameter estimation requires the application of excitation signals spanning a wide-ranging frequency spectrum, starting from a low-frequency range (fraction of a Hz) to a very high-frequency range (in the MHz range). In [16], a nine-parameter model (2RC) was used in ECM parameter estimation in the frequency domain, resulting in moderate accuracy for only certain parameter estimates. The entire frequency scanning may take close to an hour. Frequency domain approaches have been extensively employed in battery SOH studies [17,18]. The EIS-based approaches have been studied generally in laboratory settings to estimate ECM parameters [19,20] and these approaches cannot yet be used in real-life systems. Implementation of EIS in real-life battery applications requires additional hardware in order to generate and sense high-frequency excitation signals and their responses. Time domain approaches, on the other hand, can be implemented without requiring special excitation signals, which will be the focus of this paper.

The literature on time domain approaches generally considers the co-estimation of ECM parameters and the SOC [21,22] of battery. For example, in [23], parameter estimation for four different equivalent models of the battery, that represent typical battery operation modes, were discussed. For the four models, joint linear parameter estimation and SOC tracking framework were proposed. This approach is faced with dependencies on the knowledge of k-parameters of the open-circuit voltage (OCV)—the state of charge representation, i.e., OCV-SOC parameters of the battery. Additionally, the estimation of SOC is usually subject to errors in SOC initialization, integration and uncertainty in the knowledge of battery capacity. Such SOC errors consequently translate to errors in the estimation of ECM parameters using the co-estimation approach. The persistence of these errors can also be seen in methods that model battery parameters as a function of the SOC [24]. When the internal battery impedances are modelled as a function of the SOC, an extended Kalman filter (EKF) is generally implemented to jointly estimate SOC and the other battery parameters. Further, different identification methods such as the EKF, particle swarm optimization (PSO) and recursive least square (RLS) are discussed in [25] to estimate the battery's internal ECM parameters along with SOC. In [26], higher accuracy is achieved by retaining initial values for less important parameters and updating the parameters relevant to SOC and SOH estimation. It can be said that time-domain approaches to estimating ECM model parameters of a battery, without requiring other battery state information, remain sparse. In [27], an approach to independently estimate ECM parameters without requiring the SOC is proposed, where the observation model was developed based on the differentials of voltage and current measurements. However, the possibility of estimation of OCV as one of the parameters is not considered. Further, theoretical performance bounds in the accuracy of estimation were not derived.

Cramer–Rao lower bound (CRLB) defines the theoretical minimum estimation error variance, i.e., the theoretical performance bound that an estimator can achieve. In this paper, it is shown that the CRLB of estimation has a dependency on the choice of current profile for accurate estimation of internal open-circuit voltage and resistance of the battery. Using this, better approaches can be developed for ECM parameter estimation by optimizing the voltage-current profiles. Different works on ECM parameter estimation have considered different current profiles for the estimation of battery parameters [28]. However, in these works, it is neither shown that the profiles are optimal for the estimation of parameters nor is an approach to relating the estimation accuracy to the preferred current profile derived.

The contributions of the present paper are as follows:

- *ECM parameter estimation without the knowledge of SOC:* In this paper, ECM parameter estimation is formulated as a linear least squares estimation problem. Using the proposed approach, the internal open circuit voltage and the ECM parameters can be estimated without depending on the OCV-SOC model parameters and the SOC estimation algorithms, which are potential sources of errors that can eventually affect the identification of the battery's internal impedance. The developed approach is a simplistic model in terms of the voltage and current measurements from a battery.

- *Theoretical performance analysis:* The theoretical analysis is completed for the proposed approach using the theoretical bounds of estimation Cramer–Rao lower bound (CRLB). The CRLB defines the relationship of the estimation accuracy with regard to the measurement noise characteristics, the number of observations and the current profile.
- *Current profile optimization or improved estimation accuracy:* It is shown in this paper that the CRLB takes a simplified closed form for the simple R-int model of the battery. While it is known that the estimation accuracy improves with lower measurement noise variance and more observations, avenues are opened to explore current profiles that minimize the CRLB of estimation.
- *Optimization approach to select the current profile:* For the first time, an optimization approach is developed that describes the selection of current profiles to improve the accuracy of estimation. It is shown that a pulse current of equal charging and discharging magnitude minimizes the CRLB in the estimation of both the internal open circuit voltage and the internal resistance of the R-int model of the battery.

The approach presented in this paper is demonstrated using a battery simulator developed in MATLAB and validated on experimental data collected from a commercial battery.

The remainder of the paper is structured as follows: In Section 2, the mathematical derivation of the new measurement model that is based only on the measured voltage and current through the battery is presented. In Section 3, the derivation of the measurement model is extended to different model orders. Section 4 describes the proposed parameter estimation method and Section 5 contains the theoretical performance analysis of the proposed method. Section 6 summarizes the results of the testing approaches for simulated and real data. Section 7 concludes the paper.

2. Signal Model of a Battery

Figure 1 shows four different approximations of an ECM to be considered in this paper. Model 1 represents a short-circuited battery; a detailed analysis of Model 1 parameter estimation can be found in [5]. Model 2 represents the R-int model and is the subject of this paper. Models 3 and 4 represent higher-order and more accurate representations of a battery. Unlike Models 1 and 2, the optimal linear approach to parameter estimation is not feasible in Models 2 and 3. The derivations presented in this section are based on the most general model shown in Figure 1d. Section 3 shows how these derivations can be applied to the other three models.

The measured current through the battery is written as

$$z_i[k] = i[k] + n_i[k] \tag{1}$$

where $i[k]$ is the true current through the battery and $n_i[k]$ is the current measurement noise which is assumed to be zero mean and has a standard deviation (s.d.) σ_i. The measured voltage across the battery is

$$z_v[k] = v[k] + n_v[k] \tag{2}$$

where $v[k]$ is the true voltage across the battery and $n_v[k]$ is the voltage measurement noise which is assumed to be zero mean with s.d. σ_v.

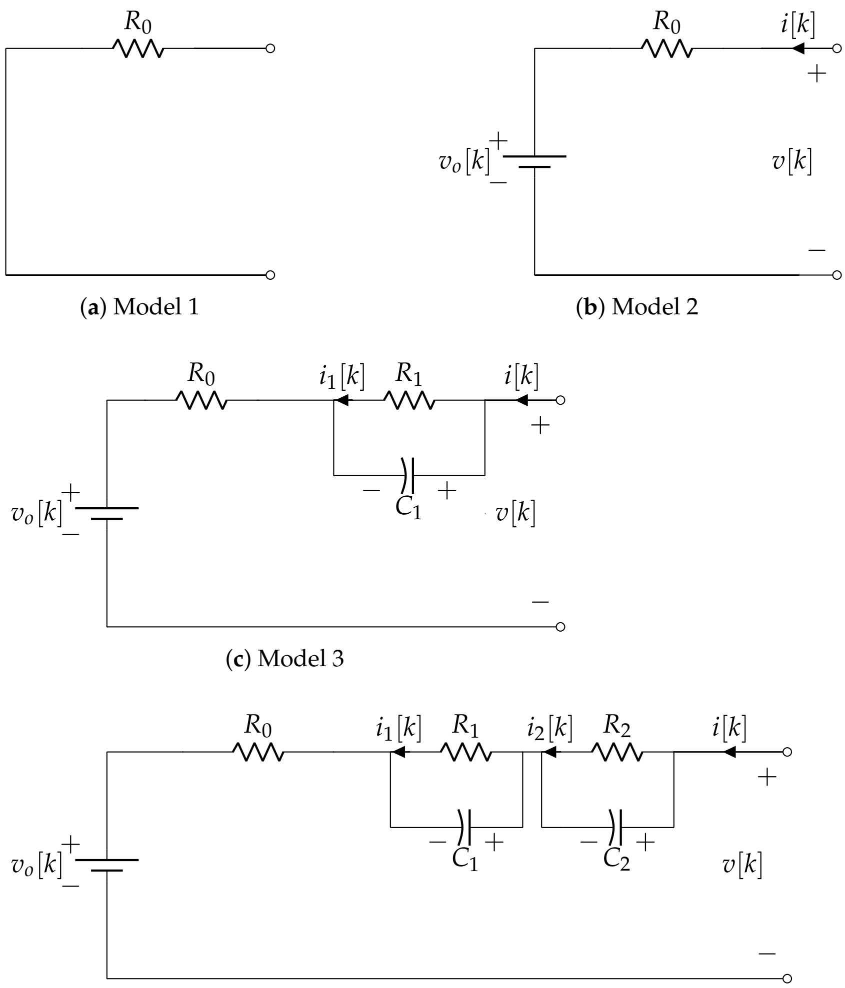

(**a**) Model 1 (**b**) Model 2

(**c**) Model 3

(**d**) Model 4

Figure 1. Different equivalent circuit model (ECM) orders. (**a**) Series resistance only. (**b**) Series resistance and battery. (**c**) Series resistance, the battery and a single RC circuit. (**d**) Series resistance, the battery and two RC circuits.

For the ECM model in Figure 1d, the true voltage across the battery, $v[k]$, is written as the sum of the voltage drop across the internal components, R_0, R_1, R_2 and the EMF, $v_o[k]$. Hence, (2), can be rewritten as,

$$z_v[k] = i[k]R_0 + x_{i_1}[k]R_1 + x_{i_2}[k]R_2 + v_o[k] + n_v[k] \tag{3}$$

where the currents through the resistors R_1 and R_2 can be written in the following form

$$x_{i_1}[k+1] \triangleq i_1[k+1] = \alpha_1 i_1[k] + (1-\alpha_1)i[k] \tag{4}$$

$$x_{i_2}[k+1] \triangleq i_2[k+1] = \alpha_2 i_2[k] + (1-\alpha_2)i[k] \tag{5}$$

where

$$\alpha_1 \triangleq e^{-\frac{\Delta}{R_1 C_1}} \tag{6}$$

$$\alpha_2 \triangleq e^{-\frac{\Delta}{R_2 C_2}} \tag{7}$$

and Δ is the sampling interval. By substituting the measured current $z_i[k]$ for $i[k]$, the currents in (4) and (5) can be rewritten as follows

$$x_{i_1}[k+1] = \alpha_1 x_{i_1}[k] + (1-\alpha_1)z_i[k] - (1-\alpha_1)n_i[k] \tag{8}$$
$$x_{i_2}[k+1] = \alpha_2 x_{i_2}[k] + (1-\alpha_2)z_i[k] - (1-\alpha_2)n_i[k] \tag{9}$$

Now, using (1), (3) can be rewritten in the z domain as follows

$$Z_v[z] = Z_i[z]R_0 + X_{i_1}[z]R_1 + X_{i_2}[z]R_2 + V_o[z] + N_v[z] - R_0 N_i[z] \tag{10}$$

Next, let us rewrite (8) in the z domain

$$zX_{i_1}[z] = \alpha_1 X_{i_1}[z] + (1-\alpha_1)Z_i[z] - (1-\alpha_1)N_i[z] \tag{11}$$

which yields

$$X_{i_1}[z] = \frac{1-\alpha_1}{z-\alpha_1}\Big(Z_i[z] - N_i[z]\Big) \tag{12}$$

and similarly for (9),

$$X_{i_2}[z] = \frac{1-\alpha_2}{z-\alpha_2}\Big(Z_i[z] - N_i[z]\Big) \tag{13}$$

By substituting (12) and (13) into (10), one gets

$$\begin{aligned} Z_v[z] = Z_i[z]R_0 + \frac{1-\alpha_1}{z-\alpha_1}Z_i[z]R_1 + \frac{1-\alpha_2}{z-\alpha_2}Z_i[z]R_2 + V_o[z] \\ + N_v[z] - \left(R_0 + \frac{1-\alpha_1}{z-\alpha_1}R_1 + \frac{1-\alpha_2}{z-\alpha_2}R_2\right)N_i[z] \end{aligned} \tag{14}$$

Rearranging (14) and converting it back to the time domain, we get

$$\begin{aligned} z_v[k] =& \alpha z_v[k-1] - \beta z_v[k-2] + R_0 z_i[k] - \check{R}_1 z_i[k-1] \\ &+ \check{R}_2 z_i[k-2] + V_o[k] + \bar{n}_i[k] + \bar{n}_v[k] \end{aligned} \tag{15}$$

where

$$\begin{aligned} \alpha &= \alpha_1 + \alpha_2 \\ \beta &= \alpha_1\alpha_2 \\ \check{R}_1 &= (\alpha_1+\alpha_2)R_0 - (1-\alpha_1)R_1 - (1-\alpha_2)R_2 \\ \check{R}_2 &= \alpha_1\alpha_2 R_0 - \alpha_2(1-\alpha_1)R_1 - \alpha_1(1-\alpha_2)R_2, \\ V_o[k] &= v_o[k] - \alpha v_o[k-1] + \beta v_o[k-2] \\ \bar{n}_v[k] &= n_v[k] - \alpha n_v[k-1] + \beta n_v[k-2] \\ \bar{n}_i[k] &= -R_0 n_i[k] + \check{R}_1 n_i[k-1] - \check{R}_2 n_i[k-2] \end{aligned}$$

Consider $V_o[k]$ to be constant over a small window of time k; then, $V_o[k] \approx V_o$. Therefore, (15) can rewritten as

$$\begin{aligned} z_v[k] =& \alpha z_v[k-1] - \beta z_v[k-2] + R_0 z_i[k] - \check{R}_1 z_i[k-1] \\ &+ \check{R}_2 z_i[k-2] + V_o + \bar{n}_i[k] + \bar{n}_v[k] \end{aligned} \tag{16}$$

Now, let us rewrite (16) in the following form

$$z_v[k] = \mathbf{a}[k]^T\mathbf{b} + n_D[k] \tag{17}$$

where the observation model $\mathbf{a}[k]^T$ and the model parameter vector $\mathbf{b}$ for the ECM model are given by

$$\begin{aligned}
&\mathbf{a}[k]^T = \mathbf{a}_4[k]^T \\
&\triangleq \Big[z_v[k-1] \quad -z_v[k-2] \quad z_i[k] \quad -z_i[k-1] \quad z_i[k-2] \quad 1 \Big]
\end{aligned} \tag{18}$$

$$\begin{aligned}
&\mathbf{b} = \mathbf{b}_4 \\
&\triangleq [\alpha \quad \beta \quad R_0 \quad \check{R}_1 \quad \check{R}_2 \quad V_o]^T
\end{aligned} \tag{19}$$

The subscripts 4 in (18) and (19) indicate that the model corresponds to Model 4, as in Figure 1d. Equivalent circuit models 1–3 are discussed later in Section 3. The noise in the voltage drop in (17) is written as

$$n_D[k] \triangleq \bar{n}_i[k] + \bar{n}_v[k] \tag{20}$$

which has the following autocorrelation

$$R_{n_D}(l) = E(n_D[k]n_D[k-l]) \tag{21}$$

This autocorrelation $R_{n_D}(l)$ for different values of l are given below:

$$\begin{aligned}
R_{n_D}(0) &= E\Big\{ n_D[k]n_D[k] \Big\} \\
&= E\Big\{ \Big\{ n_v^2[k] + \alpha^2 n_v^2[k-1] + \beta^2 n_v^2[k-2] \\
&\qquad + R_0^2 n_i^2[k] + \check{R}_1^2 n_i^2[k-1] + \check{R}_2^2 n_i^2[k-2] \Big\} \Big\} \\
&= (1+\alpha^2+\beta^2)\sigma_v^2 + (R_0^2 + \check{R}_1^2 + \check{R}_2^2)\sigma_i^2
\end{aligned} \tag{22}$$

$$\begin{aligned}
R_{n_D}(1) &= E\Big\{ n_D[k]n_D[k-1] \Big\} \\
&= E\Big\{ \Big(-\alpha n_v[k-1] + \beta n_v[k-2] + \check{R}_1 n_i[k-1] \\
&\qquad - \check{R}_2 n_i[k-2] \Big) \Big(n_v[k-1] - \alpha n_v[k-2] \\
&\qquad - R_0 n_i[k-1] + \check{R}_1 n_i[k-2] \Big) \Big\} \\
&= -\alpha(1+\beta)\sigma_v^2 - \check{R}_1(R_0 + \check{R}_2)\sigma_i^2
\end{aligned} \tag{23}$$

$$\begin{aligned}
R_{n_D}(2) &= E\Big\{ n_D[k]n_D[k-2] \Big\} \\
&= E\Big\{ \Big(\beta n_v[k-2] - \check{R}_2 n_i[k-2] \Big) \\
&\qquad \Big(n_v[k-2] - R_0 n_i[k-2] \Big) \Big\} \\
&= \beta\sigma_v^2 + R_0\check{R}_2\sigma_i^2
\end{aligned} \tag{24}$$

All the noise auto-correlation values can be summarized as follows:

$$R_{n_D}(l) \triangleq E\Big\{ n_D[k]n_D[k-l] \Big\} = \begin{cases} (1+\alpha^2+\beta^2)\sigma_v^2 + (R_0^2+\check{R}_1^2+\check{R}_2^2)\sigma_i^2 & |l| = 0 \\ -\alpha(1+\beta)\sigma_v^2 - \check{R}_1(R_0+\check{R}_2)\sigma_i^2 & |l| = 1 \\ \beta\sigma_v^2 + R_0\check{R}_2\sigma_i^2 & |l| = 2 \\ 0 & |l| > 2 \end{cases} \tag{25}$$

3. ECM Identification of Different Model Orders

The four models are explained below:

- Model 1: A series resistance only (Figure 1a).

- Model 2: A series resistance and the battery (Figure 1b).
- Model 3: A series resistance, the battery and a single RC circuit (Figure 1c).
- Model 4: A series resistance, the battery and two RC circuits (Figure 1d).

The measured voltage of each of the four equivalent circuit models shown in Figure 1 can be written in the following form:

$$z_v[k] = \mathbf{a}[k]^T \mathbf{b} + n_D[k] \tag{26}$$

where

$$\mathbf{a}[k]^T = \begin{cases} \mathbf{a}_1^T[k] & \text{Model 1} \\ \mathbf{a}_2^T[k] & \text{Model 2} \\ \mathbf{a}_3^T[k] & \text{Model 3} \\ \mathbf{a}_4^T[k] & \text{Model 4} \end{cases} \quad \mathbf{b} = \begin{cases} \mathbf{b}_1 & \text{Model 1} \\ \mathbf{b}_2 & \text{Model 2} \\ \mathbf{b}_3 & \text{Model 3} \\ \mathbf{b}_4 & \text{Model 4} \end{cases} \tag{27}$$

where

$$\mathbf{a}_1^T[k] = z_i[k] \qquad \mathbf{a}_2^T[k] = [z_i[k] \;\; 1]$$
$$\mathbf{a}_3^T[k] = \left[z_v[k-1] \;\; z_i[k] \;\; -z_i[k-1] \;\; 1\right]$$
$$\mathbf{a}_4^T[k] = \left[z_v[k-1] \;\; -z_v[k-2] \;\; z_i[k] \;\; -z_i[k-1] \;\; z_i[k-2] \;\; 1\right]$$
$$\mathbf{b}_1 = R_0 \qquad \mathbf{b}_2 = [R_0 \;\; V_o]^T$$
$$\mathbf{b}_3 = \left[\alpha_1 \;\; R_0 \;\; \check{R}_1 \;\; V_o\right]^T \qquad \mathbf{b}_4 = \left[\alpha \;\; \beta \;\; R_0 \;\; \check{R}_1 \;\; \check{R}_2 \;\; V_o\right]^T$$

For each of the above model complexities, the noise term $n_D[k]$ is expressed in terms of $\bar{n}_i[k]$ and $\bar{n}_v[k]$ as follows:

$$\bar{n}_v[k] = \begin{cases} \bar{n}_{v1}[k] & \text{Model 1} \\ \bar{n}_{v2}[k] & \text{Model 2} \\ \bar{n}_{v3}[k] & \text{Model 3} \\ \bar{n}_{v4}[k] & \text{Model 4} \end{cases} \quad \bar{n}_i[k] = \begin{cases} \bar{n}_{i1}[k] & \text{Model 1} \\ \bar{n}_{i2}[k] & \text{Model 2} \\ \bar{n}_{i3}[k] & \text{Model 3} \\ \bar{n}_{i4}[k] & \text{Model 4} \end{cases} \tag{28}$$

where

$$\bar{n}_{v1}[k] = \bar{n}_{v2}[k] = n_v[k]$$
$$\bar{n}_{v3}[k] = n_v[k] - \alpha_1 n_v[k-1]$$
$$\bar{n}_{v4}[k] = n_v[k] - (\alpha_1 + \alpha_2) n_v[k-1] + \alpha_1 \alpha_2 n_v[k-2]$$
$$\bar{n}_{i1}[k] = \bar{n}_{i2}[k] = -R_0 n_i[k]$$
$$\bar{n}_{i3}[k] = -R_0 n_i[k] + \check{R}_1 n_i[k-1]$$
$$\bar{n}_{i4}[k] = -R_0 n_i[k] + \check{R}_1 n_i[k-1] - \check{R}_2 n_i[k-2]$$

The autocorrelation for all four model orders is as follows:

$$R_{n_D}(0) = E\left\{n_D[k] n_D[k]\right\} = \begin{cases} \sigma_v^2 + R_0^2 \sigma_i^2 & \text{Model 1} \\ \sigma_v^2 + R_0^2 \sigma_i^2 & \text{Model 2} \\ (1+\alpha_1^2)\sigma_v^2 + \left(R_0^2 + \check{R}_1^2\right)\sigma_i^2 & \text{Model 3} \\ (1+\alpha^2+\beta^2)\sigma_v^2 + \left(R_0^2 + \check{R}_1^2 + \check{R}_2^2\right)\sigma_i^2 & \text{Model 4} \end{cases} \tag{29}$$

$$R_{n_D}(1) = E\Big\{n_D[k]n_D[k-1]\Big\} = \begin{cases} 0 & \text{Model } 1 \\ 0 & \text{Model } 2 \\ -\alpha_1\sigma_v^2 - R_0\check{R}_1\sigma_i^2 & \text{Model } 3 \\ -\alpha(1+\beta)\sigma_v^2 - \check{R}_1(R_0+\check{R}_2)\sigma_i^2 & \text{Model } 4 \end{cases} \tag{30}$$

$$R_{n_D}(2) = E\Big\{n_D[k]n_D[k-2]\Big\} = \begin{cases} 0 & \text{Model } 1 \\ 0 & \text{Model } 2 \\ 0 & \text{Model } 3 \\ \beta\sigma_v^2 + R_0\check{R}_2\sigma_i^2 & \text{Model } 4 \end{cases} \tag{31}$$

The auto-correlation $R_{n_D}(l)$ is zero when $l > 2$ for all four models.

4. Parameter Estimation Method

The measurements are grouped into batches of equal length L_b. Using (26), the vector observation model is rewritten for a particular batch of data of length L_b.

$$\mathbf{z}_v[\kappa] = \mathbf{H}[\kappa]^T\mathbf{b} + \mathbf{n}_D[\kappa] \tag{32}$$

where κ denotes the batch number,

$$\mathbf{z}_v[\kappa] = \begin{bmatrix} z_v[(\kappa-1)L_b+1] \\ z_v[(\kappa-1)L_b+2] \\ \vdots \\ z_v[\kappa L_b] \end{bmatrix}, \ \mathbf{n}_D[\kappa] = \begin{bmatrix} n_D[(\kappa-1)L_b+1] \\ n_D[(\kappa-1)L_b+2] \\ \vdots \\ n_D[\kappa L_b] \end{bmatrix}$$

$$\mathbf{H}[\kappa] = \begin{bmatrix} \mathbf{a}[(\kappa-1)L_b+1] \\ \mathbf{a}[(\kappa-1)L_b+2] \\ \vdots \\ \mathbf{a}[\kappa L_b] \end{bmatrix}, \ \mathbf{a}[k]^T = \begin{cases} \mathbf{a}_1^T[k] & \text{Model 1} \\ \mathbf{a}_2^T[k] & \text{Model 2} \\ \mathbf{a}_3^T[k] & \text{Model 3} \\ \mathbf{a}_4^T[k] & \text{Model 4} \end{cases}$$

The correlation matrix of the noise vector $\mathbf{n}_D[\kappa]$ is written as

$$E\Big(\mathbf{n}_D[\kappa]\mathbf{n}_D[\kappa]^T\Big) = \mathbf{R}_{\mathbf{n}_D}[\kappa] \tag{33}$$

where $\mathbf{R}_{\mathbf{n}_D}[\kappa]$ is a banded symmetric Toeplitz matrix which is diagonal for Models 1 and 2, tridiagonal for Model 3 and pentadiagonal for Model 4. The diagonal entry of $\mathbf{R}_{\mathbf{n}_D}[\kappa]$ is given by $R_{n_D}(1)$, the first off-diagonal entry is given by $R_{n_D}(1)$ and the second off-diagonal entry is given by $R_{n_D}(2)$ in (29) to (31). All the other off-diagonal elements of $\mathbf{R}_{\mathbf{n}_D}[\kappa]$ are zero.

Given the κ^{th} batch of observations, the least square (LS) estimate of $\mathbf{b}$ can be written as

$$\hat{\mathbf{x}}_{\text{LS}}[\kappa] = \Big(\mathbf{H}[\kappa]^T\mathbf{R}_{\mathbf{n}_D}[\kappa]^{-1}\mathbf{H}[\kappa]\Big)^{-1}\mathbf{H}[\kappa]^T\mathbf{R}_{\mathbf{n}_D}[\kappa]^{-1}\mathbf{z}_v[\kappa] \tag{34}$$

It can be shown that the covariance of the LS estimation error is

$$P[\kappa] = \Big(\mathbf{H}[\kappa]^T\mathbf{R}_{\mathbf{n}_D}[\kappa]^{-1}\mathbf{H}[\kappa]\Big)^{-1} \tag{35}$$

When the parameter $\mathbf{b}$ needs to be estimated using more data, the batch length L_b increases, resulting in significantly high computational complexity. Rather than increasing L_b, a recursive least square (RLS) algorithm can be employed to achieve the same performance without significantly increasing computational load. Algorithm 1 summarizes one iteration of the RLS algorithm. The input to this algorithm is the estimate $\hat{\mathbf{x}}[\kappa]$ and the error covariance $\mathbf{P}[\kappa]$ from the prior batch, the new measurement $\mathbf{z}[\kappa+1]$ and the new measurement model $\mathbf{H}[\kappa+1]$. The outputs are the new estimate $\hat{\mathbf{x}}[\kappa+1]$ and the updated error covariance $\mathbf{P}[\kappa+1]$.

Algorithm 1 $\left[\hat{\mathbf{x}}[\kappa+1], \mathbf{P}[\kappa+1]\right] = \mathrm{RLS}[\hat{\mathbf{x}}[\kappa], \mathbf{P}[\kappa], \mathbf{H}[\kappa+1], \mathbf{z}[\kappa+1]]$

1: Update residual covariance:
$\mathbf{S}[\kappa+1] = \mathbf{H}[\kappa+1]\mathbf{P}[\kappa]\mathbf{H}[\kappa+1]^T + \mathbf{R}[\kappa+1]$
2: Update gain:
$\mathbf{W}[\kappa+1] = \mathbf{P}[\kappa]\mathbf{H}[\kappa+1]^T\mathbf{S}[\kappa+1]^{-1}$
3: Update parameter:
$\hat{\mathbf{x}}[\kappa+1] = \hat{\mathbf{x}}[\kappa] + \mathbf{W}[\kappa+1](\mathbf{z}[\kappa+1] - \mathbf{H}[\kappa+1]\hat{\mathbf{x}}[\kappa])$
4: Update information:
$\mathbf{P}^{-1}[\kappa+1] = \mathbf{P}^{-1}[\kappa] + \mathbf{H}[\kappa+1]^T\mathbf{R}[\kappa+1]^{-1}\mathbf{H}[\kappa+1]$

The calculation of the model parameters from the estimates $\hat{\mathbf{x}}_{\mathrm{LS}}[\kappa]$ is given below for Model 3. From (28), the estimate has four elements:

$$\hat{\mathbf{x}}_{\mathrm{LS}}[\kappa] = \mathbf{b}_3 = \begin{bmatrix}\alpha_1 & R_0 & \check{R}_1 & V_o\end{bmatrix}^T$$

After estimation, the parameters of the ECM Model 3, R_1 and C_1 are recovered as follows:

$$R_1 = \frac{(\check{R}_1 - \alpha_1 R_0)}{(\alpha_1 - 1)}, \qquad C_1 = \frac{-\Delta}{R_1 \ln \alpha_1}$$

5. Performance Analysis

In this section, a theoretical performance analysis of the proposed parameter estimation algorithm is developed. For linear observation model (32) under Gaussian noise assumption, the Cramer–Rao Lower Bound (CRLB) [29] serves as the lower bound on the estimation error covariance. It can be shown that, for the observation model (32), the CRLB is

$$\mathrm{CRLB} = \left(\mathbf{H}[\kappa]^T\boldsymbol{\Sigma}^{-1}\mathbf{H}[\kappa]\right)^{-1} \tag{36}$$

i.e.,

$$E\left((\hat{\mathbf{b}} - \mathbf{b})(\hat{\mathbf{b}} - \mathbf{b})^T\right) \geq \mathrm{CRLB} \tag{37}$$

where $\hat{\mathbf{b}}$ denotes an estimate of $\mathbf{b}$.

Now, let us focus on the CRLB corresponding to Model 2 in Figure 1 for an in-depth analysis. For this model, the CRLB simplifies to

$$\mathrm{CRLB} = \sigma^2\left(\mathbf{H}[\kappa]^T\mathbf{H}[\kappa]\right)^{-1} \tag{38}$$

and $\mathbf{H}[\kappa]^T\mathbf{H}[\kappa]$ can be expanded as follows

$$\mathbf{H}[\kappa]^T\mathbf{H}[\kappa] = \begin{bmatrix}\sum_{k=1}^{L} i(k)^2 & \sum_{k=1}^{L} i(k) \\ \sum_{k=1}^{L} i(k) & L\end{bmatrix} \tag{39}$$

where $\mathbf{z}_i(k) = i(k)$ is assumed in order to simplify the analysis.

Now, $\left(\mathbf{H}[\kappa]^T\mathbf{H}[\kappa]\right)^{-1}$ can be simplified as

$$\left(\mathbf{H}[\kappa]^T\mathbf{H}[\kappa]\right)^{-1} = \left(\frac{1}{|\mathbf{H}[\kappa]^T\mathbf{H}[\kappa]|}\right)\begin{bmatrix}L & -\sum_{k=1}^{L} i(k) \\ -\sum_{k=1}^{L} i(k) & \sum_{k=1}^{L} i(k)^2\end{bmatrix} \tag{40}$$

where

$$\left|\mathbf{H}[\kappa]^T\mathbf{H}[\kappa]\right| = L\sum_{k=1}^{L} i(k)^2 - \left(\sum_{k=1}^{L} i(k)\right)^2 \tag{41}$$

From the above, the CRLB of estimating R_0 and V_o, the first and second diagonal elements, respectively, of (38) can be written as

$$\mathrm{CRLB}(R_0) = \frac{\sigma^2}{\sum_{k=1}^{L} i(k)^2 - \frac{1}{L}\left(\sum_{k=1}^{L} i(k)\right)^2} \tag{42}$$

$$\mathrm{CRLB}(V_o) = \frac{(\sigma^2/L)\sum_{k=1}^{L} i(k)^2}{\sum_{k=1}^{L} i(k)^2 - \frac{1}{L}\left(\sum_{k=1}^{L} i(k)\right)^2} = \left(\frac{\sigma^2}{L}\right)\left(\frac{1}{1-\frac{1}{L}\left(\frac{\left(\sum_{k=1}^{L} i(k)\right)^2}{\sum_{k=1}^{L} i(k)^2}\right)}\right) \tag{43}$$

In other words, one can write

$$E\left((\hat{R}_0 - R_0)^2\right) \geq \mathrm{CRLB}(R_0) \tag{44}$$

$$E\left((\hat{V}_o - V_o)^2\right) \geq \mathrm{CRLB}(V_o) \tag{45}$$

Let us first consider $\mathrm{CRLB}(R_0)$ in (42). The estimation accuracy depends on the following three factors:

(1) *Measurement noise variance* σ^2. The lower the measurement noise, the lower the CRLB.
(2) *Number of observations* L. Under the given assumptions, that R_0 remains a constant, more measurements will decrease estimation error.
(3) *Current profile* $i(k),\ k = 1, \ldots, L$. The current profile should be selected in a way that the error bound in (42) is minimized.

Out of the three factors influencing the estimation error of R_0, two are constants. The current profile $i(k),\ k = 1, \ldots, L$ should be selected in a way that the error can be made as small as possible.

Remark 1. *Let us assume all the values of the current are the same, i.e.,* $i(1) = i(2) = \ldots = i(L)$*. This will make the denominator of* (42) *zero and lead to infinite error variance. Another way to look at it is that all equal values of* $i(k)$ *will make* $\mathbf{A}$ *rank deficient.*

We need to find the current profile $i(1), i(2), \ldots, i(L)$ such that the $\mathrm{CRLB}(R_0)$ can be reduced. The problem can be formally stated as follows:

Problem 1. *For a given number of measurements* L *find* $i(1), i(2), \ldots, i(L)$ *such that the following cost function is maximized:*

$$\mathcal{J}_{R_0}(i(1), i(2), \ldots, i(L)) = \sum_{k=1}^{L} i(k)^2 - \frac{1}{L}\left(\sum_{k=1}^{L} i(k)\right)^2 \tag{46}$$

under the constraint that

$$i_{\min} \leq i(1), i(2), \ldots, i(L) \leq i_{\max} \tag{47}$$

It can be shown that for given values of the current limits $i_{\min}$ and $i_{\max}$, a current profile that alternates between the two extreme values will minimize $\mathrm{CRLB}(R_0)$.

Minimization of $\mathrm{CRLB}(V_o)$ can be formulated as the following problem:

Problem 2. *For a given number of measurements L, find $i(1), i(2), \ldots, i(L)$ such that the following cost function is minimized:*

$$\mathcal{J}_{V_o}(i(1), i(2), \ldots, i(L)) = \left(\frac{\left(\sum_{k=1}^{L} i(k)\right)^2}{\sum_{k=1}^{L} i(k)^2} \right) \tag{48}$$

under the constraint that

$$i_{\min} \leq i(1), i(2), \ldots, i(L) \leq i_{\max} \tag{49}$$

Selecting current limits such that

$$i_{\min} = -i_{\max}$$

and a current profile that alternates between $i_{\min}$ and $i_{\max}$ will minimize both $\text{CRLB}(R_0)$ and $\text{CRLB}(V_o)$.

The performance analysis presented in this section shows that the accuracy of the estimation depends on the excitation signal. By carefully selecting the excitation signal, the accuracy of ECM parameter estimation can be improved. When there is no control over the excitation signal, e.g., when using battery usage data for ECM parameter estimation, the CRLB provides the lower bound on the ECM parameter estimation error.

6. Simulation Analysis

The data for the demonstration in this section were generated using a battery simulator. Figure 2 shows the battery simulator in the form of a block diagram. The battery simulator uses the equivalent circuit model shown in Figure 1 to simulate the voltage and current measurements that resemble real-time measurements from a battery. All simulation analyses in this paper were done by using MATLAB software version R2022a developed by MathWorks [30]. The OCV effect of the battery, denoted by $v_o[k]$ in Figure 1, was generated using the Combined+3 model [31] with the following model parameters: $k_0 = -9.082$, $k_1 = 103.087$, $k_2 = -18.185$, $k_3 = 2.062$, $k_4 = -0.102$, $k_5 = -76.604$, $k_6 = 141.199$, and $k_7 = -1.117$. The voltage measurements across the battery were simulated using the observation model in (3). The voltage and current measurement noises were implemented based on (2) and (1), respectively, where the voltage and current measurement noise standard deviations were assumed to be equal in magnitude, i.e., $\sigma_v = \sigma_i = \sigma$, where σ was computed based on the assumed signal-to-noise ratio of the measurement system, defined as

$$\text{SNR} = 20 \log\left(\frac{I}{\sigma}\right) \tag{50}$$

where $I = |i(k)|,\ k = 1, \ldots, L$ is the amplitude of the current signal that is assumed to be constant throughout the entire simulation. The relaxation parameters of the ECM are set at $R_0 = 0.2$, $R_1 = 0.3$, $C_1 = 50$, $R_2 = 0.3$, and $C_2 = 500$. The EECM model in the battery simulator can be changed in a way that the RC models can be selected from the set of $\{(R_0), (R_1, C_1), (R_2, C_2)\}$.

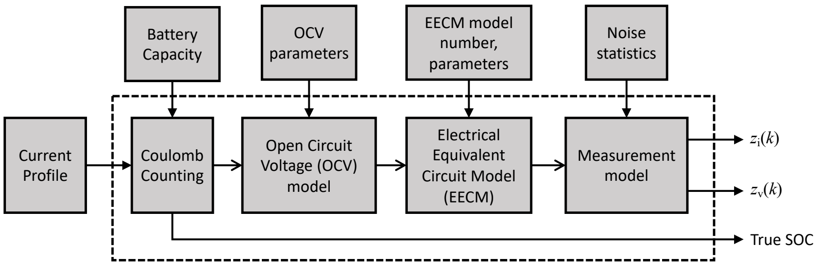

Figure 2. Battery simulator used to simulate the voltage and current measurements in this paper.

First, let us consider the current profile shown in Figure 3. The current is sampled at 10 Hz resulting in $L = 1000$ samples. The current profile $i(1), i(2), \ldots, i(L)$ also holds the following property

$$\sum_{i=1}^{L} i(k) = 0 \tag{51}$$

where $L = 1000$.

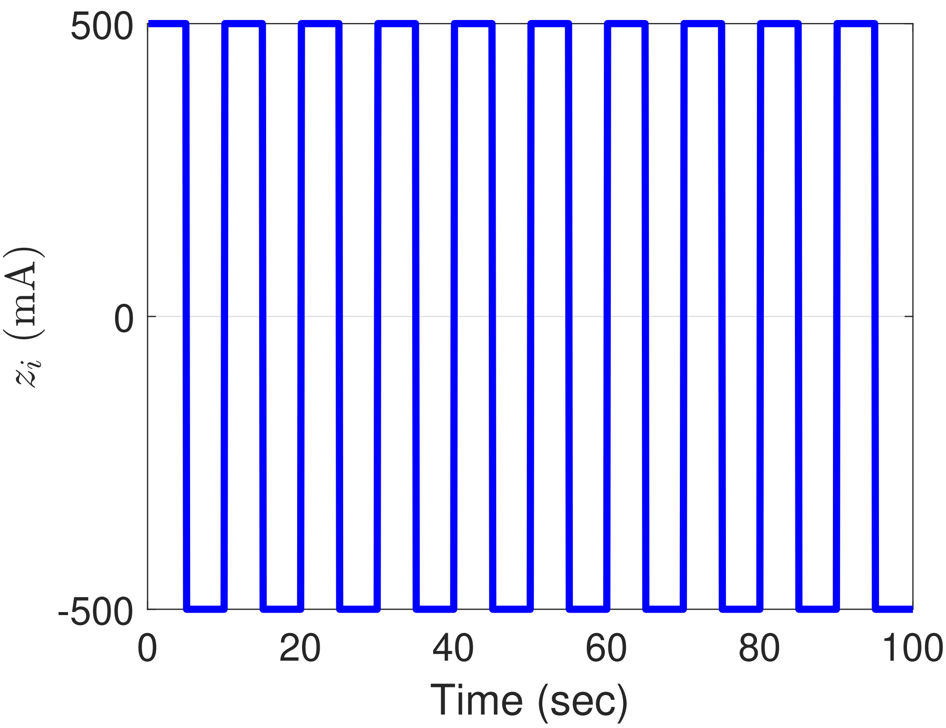

Figure 3. Current profile 1 generated using the battery simulator with constant amplitude.

Figure 4 shows a plot of OCV $V_o(k)$ over time. It can be seen that when the current $i(k)$ is positive $V_o(k)$ increases and when $i(k)$ is negative $V_o(k)$ decreases. Since the average current shown in Figure 3 is zero, the average OCV in Figure 4 is constant as well.

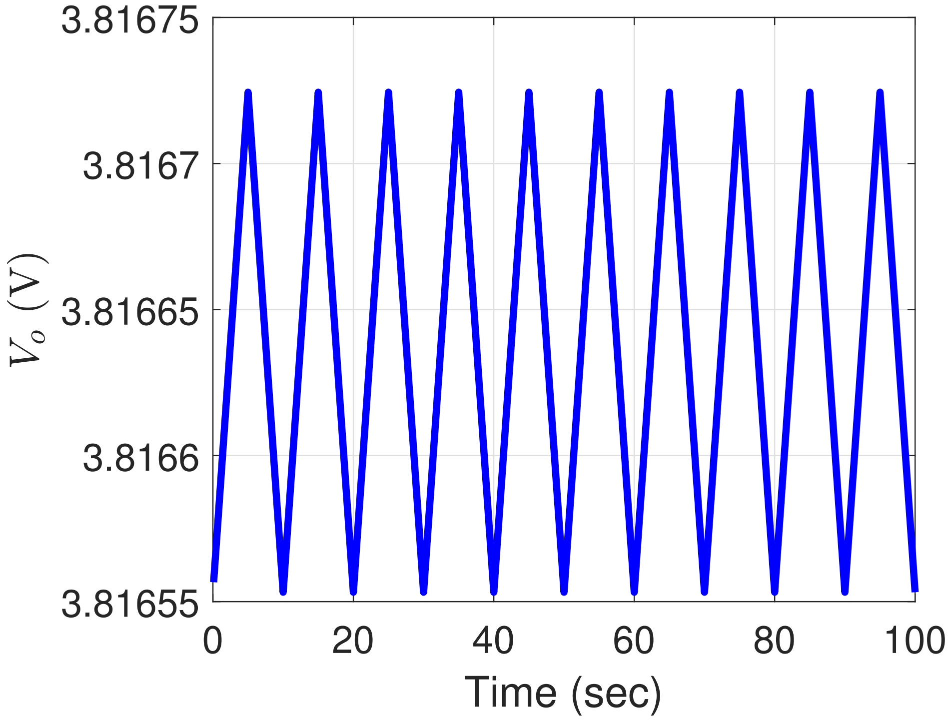

Figure 4. Simulated open circuit voltage (OCV). The average OCV is $V_o = 3.8165649$ V.

Figure 5 shows a plot of the true voltage across the battery terminals, $v(k) = V_o(k) + i(k)R_0$, over time. It must be noted that even though $V_o(k)$ changes with time, the magnitude of the voltage drop $i(k)R_0$ remains a constant. Moreover, the magnitude of change in $V_o(k)$ (see Figure 4) is relatively insignificant compared to the magnitude of $i(k)R_0$. Consequently, the magnitude of $v(k)$ appears unchanged in Figure 5. Another explanation for this observation is that the change in OCV is small within a duration of 5 s.

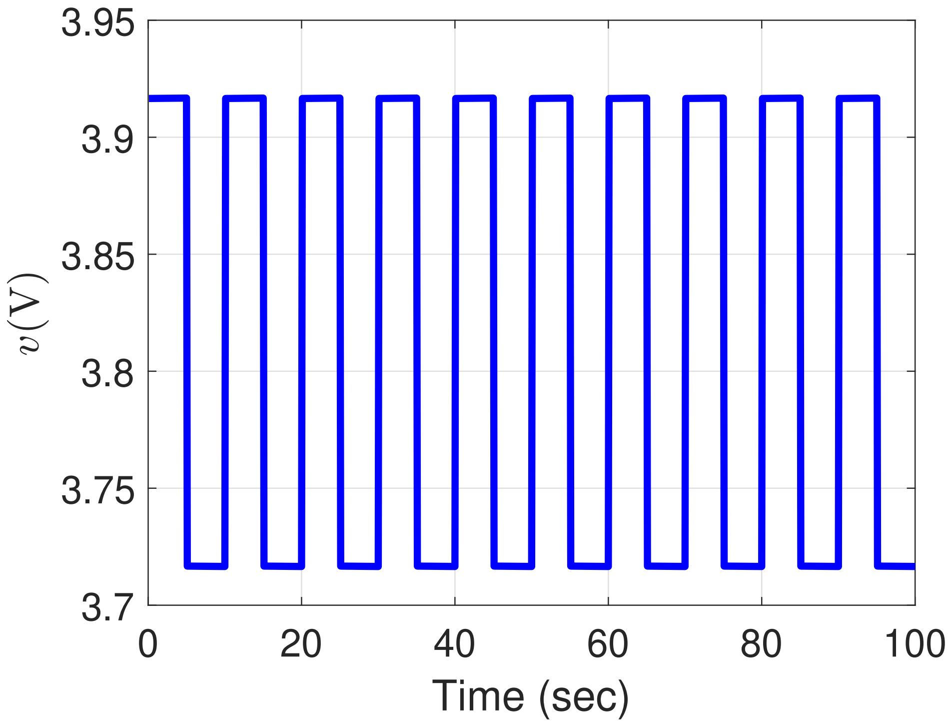

Figure 5. True voltage measurements across the battery terminals.

Figure 6 shows the voltage measurements from the battery simulator. Here, the battery simulator is set to Model 2 ECM (see Figure 1), i.e., only $R_0 = 0.2\,\Omega$ had a non-zero value and all other ECM parameters were set to zero. For now, it is assumed that the current profile is perfectly known, as shown in Figure 3; i.e., it is assumed that the current measurement noise is zero.

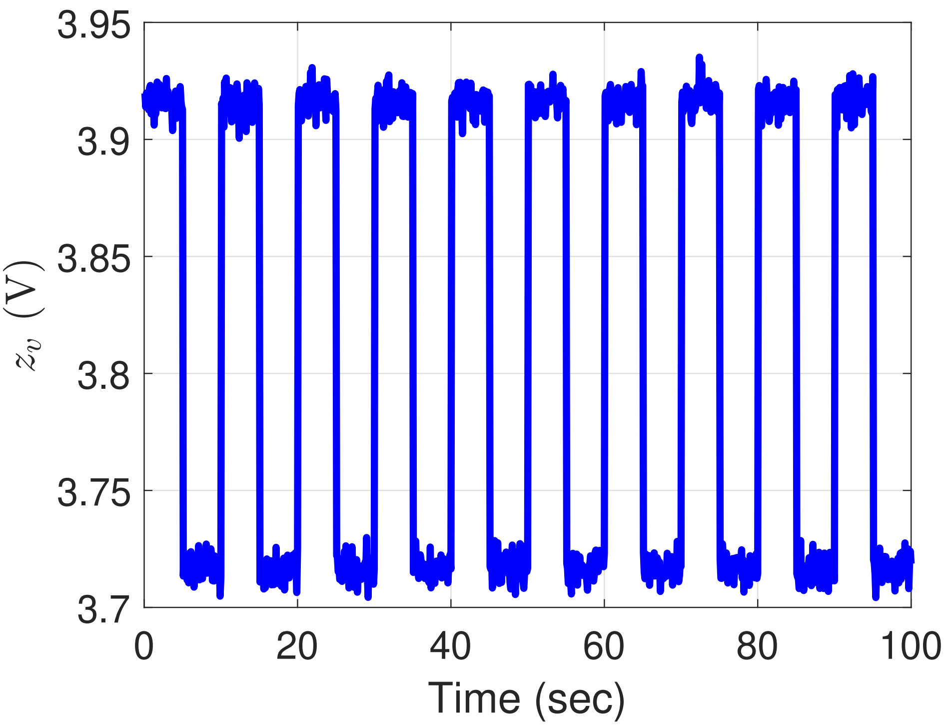

Figure 6. Voltage measurements across the battery terminals simulated using the battery simulator.

The least-square estimation algorithm (34) for Model 2 was used to estimate the resistance R_0 and V_o. Let us denote these estimated quantities as $\hat{R}_0$ and $\hat{V}_o$, respectively. The normalized mean square error (NMSE) of these estimates is defined as

$$\text{NMSE}(R_0) = \frac{1}{R_0^2} \sum_{m=1}^{M} (R_0 - \hat{R}_0(m))^2 \tag{52}$$

$$\text{NMSE}(V_o) = \frac{1}{V_o^2} \sum_{m=1}^{M} (V_o - \hat{V}_o(m))^2 \tag{53}$$

where M denotes the number of Monte-Carlo runs.

In order to make the CRLB comparable to the NMSE defined in (52) and (53), the following CRLB values in (42) and (43) were computed for comparison during simulation studies.

$$\text{CRLB}(R_0) \rightarrow \frac{\text{CRLB}(R_0)}{R_0^2} \tag{54}$$

$$\text{CRLB}(V_o) \rightarrow \frac{\text{CRLB}(V_o)}{V_o^2} \tag{55}$$

6.1. Perfect ECM Assumption

In a perfect ECM assumption, the battery management system assumes the same model as the battery simulator. We will now consider a scenario where the battery simulator and BMS assume Model 2. The NMSE for R_0 is calculated using Equation (52) where $\hat{R}_0$ for Model 2 is estimated over 1000 Monte-Carlo runs. The CRLB for R_0 is calculated using Equation (54), where the length of current samples (Figure 3) is $L = 1000$. Figure 7 shows the NMSE and CRLB for R_0 estimation under model matched assumption. It can be observed that the NMSE is close to the theoretical bound CRLB for all SNR levels indicating an efficient estimator.

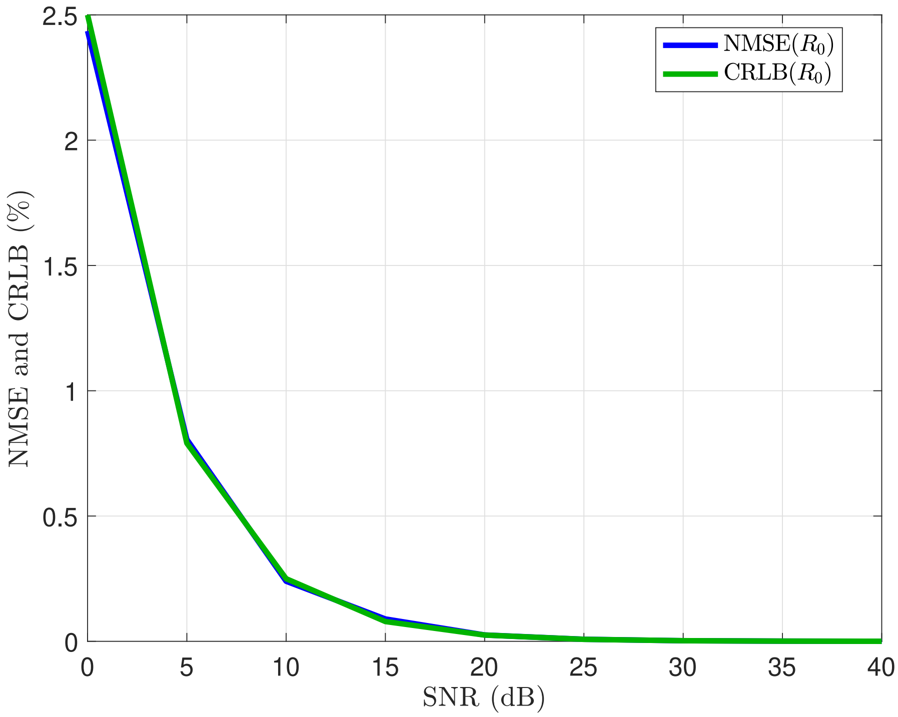

Figure 7. Performance of R_0 estimation using ECM Model 2 under perfect ECM assumption.

Similarly, in Figure 8, the NMSE of V_o estimate is plotted with CRLB of V_o for SNR values between 0 and 40 dB. The NMSE of V_o estimate is calculated using (53) and the CRLB of V_o estimate is calculated using (55). It can be observed again that the performance of the estimator is close to the theoretical bound CRLB and that the estimator is efficient.

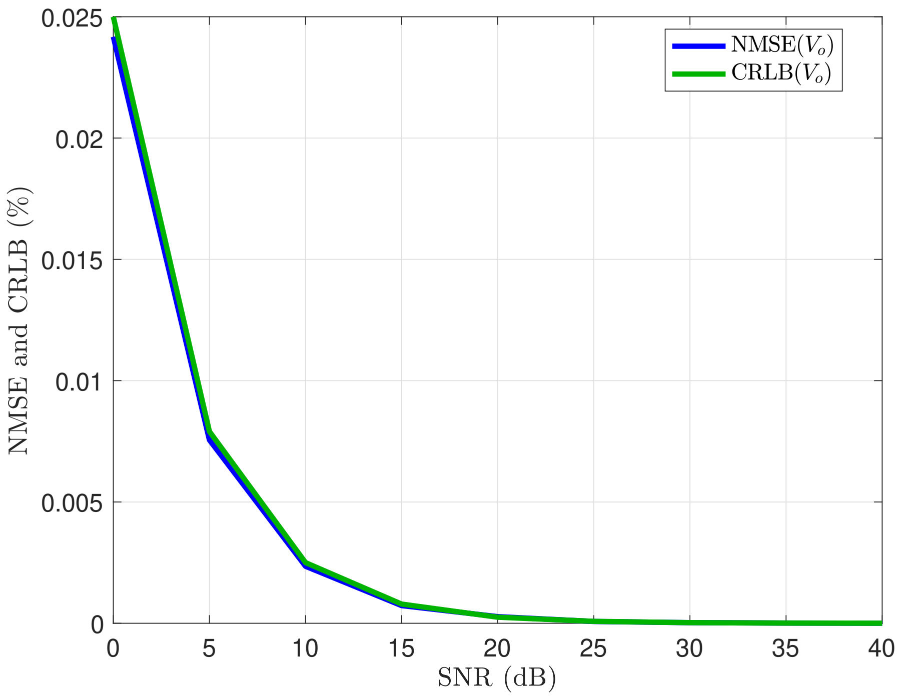

Figure 8. Performance of OCV estimation using ECM Model 2 under perfect ECM assumption.

Now, let us compare the resistance estimates under the perfect ECM assumption for a particular SNR level. Table 1 contains the R_0 estimate for Model 2 under perfect ECM assumption at SNR = 20 dB. When the BMS and battery simulator assumes Model 2, the estimate of resistance R_0 is obtained as an average from the estimate of R_0 over 1000 Monte-Carlo runs. The table also shows another case of perfect ECM assumption where the simulator, as well as the estimator, correspond to Model 3. Due to this assumption, the model parameter vector consists of two resistance R_0 and R_1 values as in Figure 1c. Thus, when the BMS and battery simulator assumes Model 3, the estimate of resistances, R_0 and R_1 are obtained as an average from the estimates of R_0 and R_1 over 1000 Monte-Carlo runs.

Table 1. Average estimates of equivalent circuit model (ECM) parameters under perfect ECM assumption (20 dB).

Battery Simulator	BMS	R_0	R_1	$\hat{R}_0$	$\hat{R}_1$
Model 2	Model 2	0.2	NA	0.1999	NA
Model 3	Model 3	0.2	0.1	0.2114	0.0740

6.2. Realistic ECM Assumption

In this section, a simulation-based ECM parameter estimation analysis is presented based on a realistic ECM assumption in which the battery management system assumes an ECM model that is different from the one used by the battery simulator to simulate the measurements. In this section, we consider a scenario where the battery simulator assumes Model 3 and the BMS assumes Model 2. It must be noted that the CRLB derivations are done under perfect model assumptions. Figure 9 shows the NMSE and CRLB computed under the model mismatch assumption. The NMSE is significantly greater than CRLB at all SNR levels. An explanation for this observation can be stated based on the model assumptions made for this simulation: ECM Model 3 contains two resistor components, R_0 and R_1. When a lower order model, here Model 2, is used to estimate the parameters, the resulting estimate of the resistance is observed to be closer to the sum of the two resistor components of Model 3. To confirm this observation, let us define a new type of NMSE as follows:

$$\mathrm{NMSE}(R_{\mathrm{tot}}) = \frac{1}{R_{\mathrm{tot}}^2} \sum_{m=1}^{M} (R_{\mathrm{tot}} - \hat{R}_0(m))^2 \tag{56}$$

Here, the estimation error is computed with respect to the total resistance, defined as $R_{\mathrm{tot}} = R_0 + R_1$. Figure 10 shows the computed NMSE based on the two different definitions given in (52) and (56). In this figure, it can be observed that $\mathrm{NMSE}(R_{\mathrm{tot}})$ is less than the NMSE for $\mathrm{NMSE}(R_0)$ at all SNR levels. This means that the BMS under the Model 2 assumption estimates both resistances together, as a summation. Thus, it can be confirmed that the estimation of resistance of ECM Model 2 is approximately the sum of the two resistor components of Model 3.

Now, let us compare the estimates of resistances under the perfect and realistic ECM assumptions at a particular SNR level. Table 2 contains the averages of the R_0 and R_1 estimates for both assumptions of ECM Model 3. The parameter estimate is obtained as an average from the estimates of 1000 Monte-Carlo runs at SNR = 20 dB. While using the realistic ECM model, the estimation algorithm assumes a different model, Model 2. Thus, from the ECM in Figure 1b, one estimate of resistance is obtained, i.e., 0.2823 Ω. Now we apply the observation that the resistance of an ECM Model 2 is approximately the sum of the two resistor components of Model 3. Conforming to this observation, the Model 2 estimate is shown to be the total resistance of ECM Model 3 $0.2114 + 0.074 \approx 0.2823$ under perfect ECM assumption.

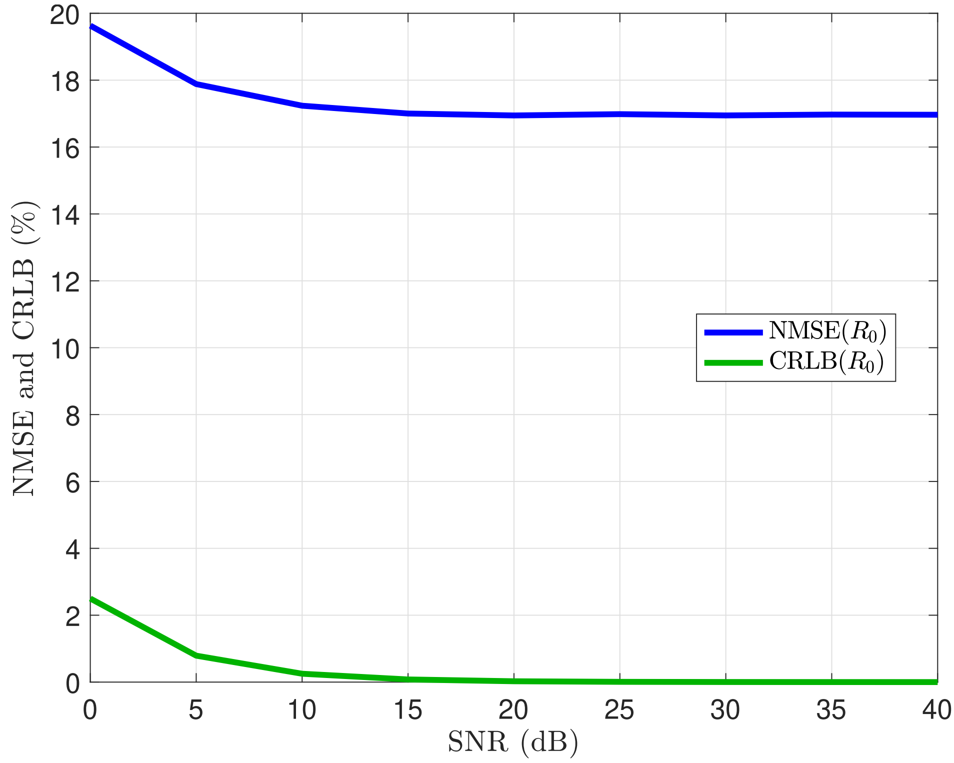

Figure 9. Performance of R_0 estimation under model mismatch assumption.

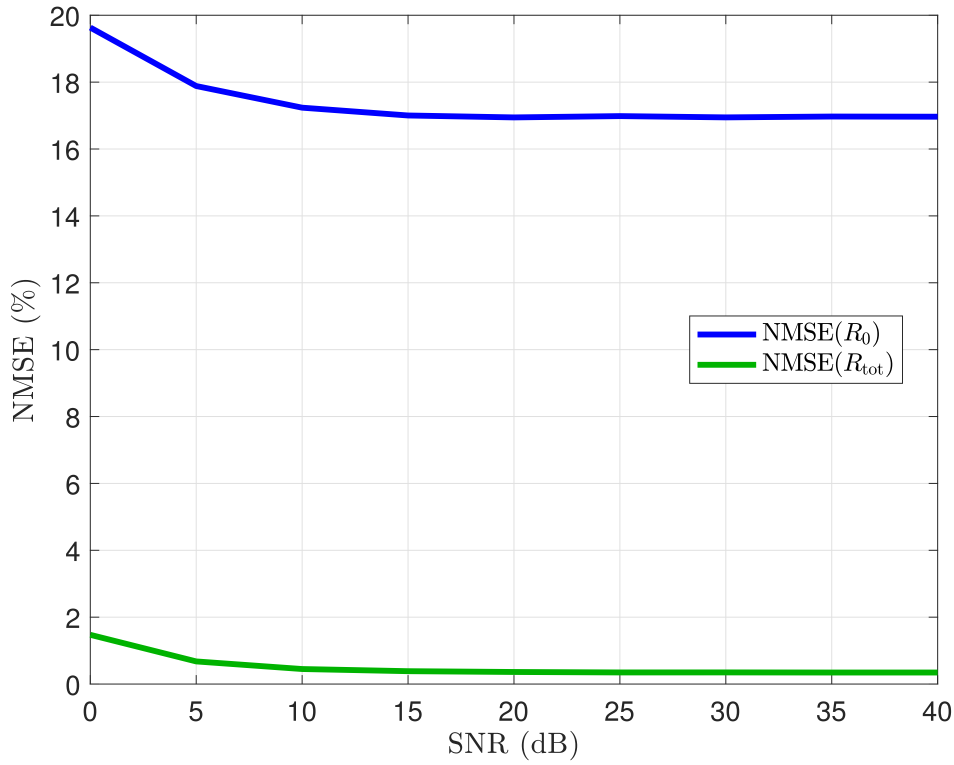

Figure 10. Performance of R_0 estimation under model mismatch assumption.

Table 2. Average Estimates of ECM Parameters under ECM model mismatch assumption (20 dB).

Battery Simulator	BMS	R_0	R_1	$\hat{R}_0$	$\hat{R}_1$
Model 3	Model 3	0.2	0.1	0.2114	0.0740
Model 3	Model 2	0.2	0.1	0.2823	NA

The simulation analysis presented in this section under realistic ECM assumption is important because of the fact that when it comes to real battery applications, the assumed model is always different from the realistic case. Moreover, most battery management systems resort to reduced order models in order to save computation and hardware complexity.

6.3. Real Data

In this subsection, the performance of the proposed approach for battery parameter estimation using data collected from a Samsung-30T INR21700 battery cell is presented. A current profile, shown in Figure 11 is applied to the battery and the voltage across the battery terminals is recorded. The data collection is performed using the Arbin BT-2000 battery cycler shown in Figure 12 and is made available in this link: https://data.mendeley.com/datasets/h3yfxtwkjz, accessed on 24 October 2022.

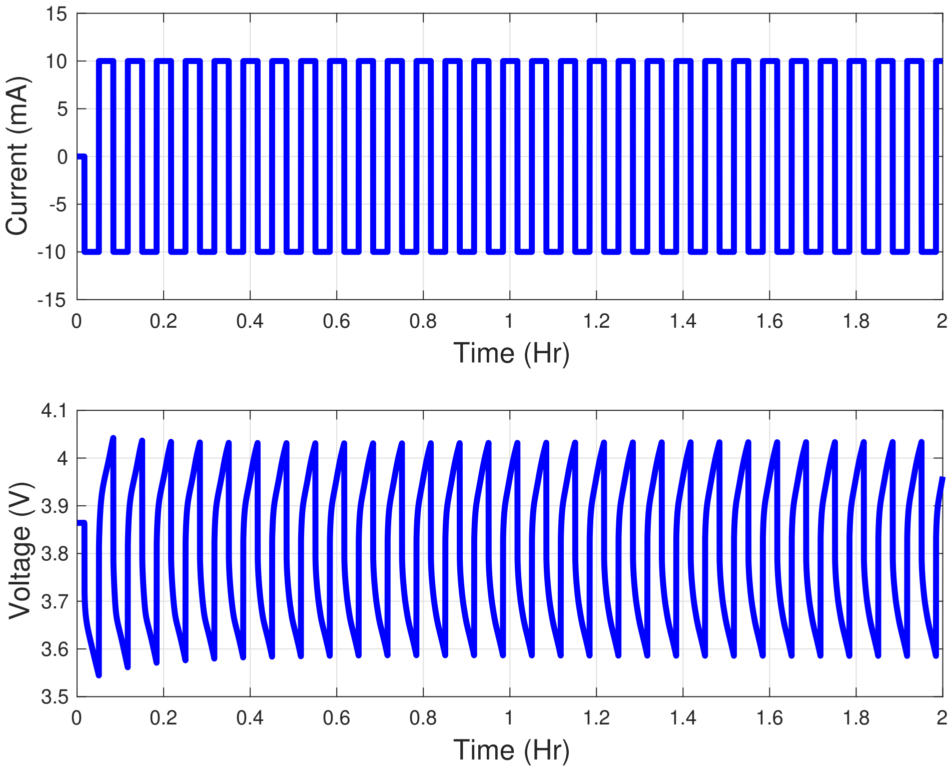

Figure 11. Current and voltage measurements collected from a real battery using a battery cycler.

The s.d. of the voltage and current measurement error of the device is approximately 0.00033 V and 0.00025 A, respectively. The sampling time of the data is $\Delta = 1$ second; this resulted in close to 7200 voltage and current measurements as shown in Figure 11. Then, least square estimation (34) is performed on the recorded data to estimate the model parameters. Table 3 shows the parameters obtained when the estimation algorithm is set to ECM Models 2 and 3, respectively. The parameter estimate is obtained as an average from the estimates over 1000 Monte-Carlo runs. Here, while using Model 2 to estimate the parameters, the resistance estimate is $\hat{R}_0 = 0.0152\,\Omega$. When Model 3 is used, the individual resistance estimates are $\hat{R}_0 = 0.0107$ and $\hat{R}_1 = 0.0049$, resulting in $\hat{R}_0 + \hat{R}_1 = 0.0152$, which is approximately equal to the Model 2 estimation of $\hat{R}_0$. Thus, the observation that while using Model 2, the resistance obtained is closer to the summation of all the resistor components of Model 3 holds true for real-battery data.

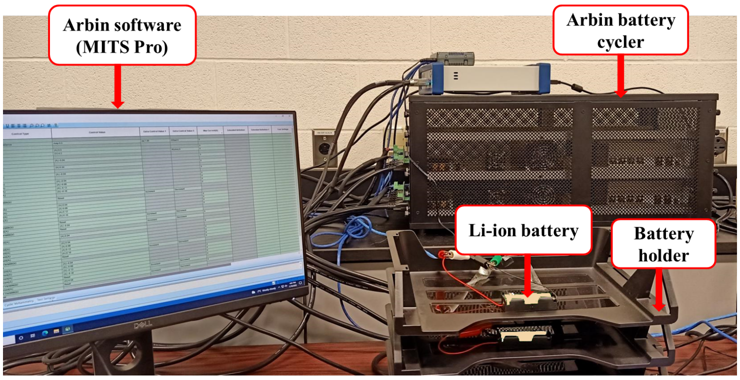

Figure 12. Experimental setup for battery testing [32].

Table 3. Estimates of ECM Parameters using the real voltage and current measurements.

BMS	$\hat{R}_0$	$\hat{R}_1$
Model 2	0.0152	NA
Model 3	0.0107	0.0049

7. Conclusions

In this paper, the Cramer–Rao Lower Bound (CRLB) of estimating the equivalent circuit model parameters of a battery is derived. It was shown that an alternating current excitation signal improves the estimation accuracy of the R-int approximation of the equivalent circuit model. It was shown using simulation studies that the R-int approximation can be efficient; that is, the estimation error variance becomes the same as the CRLB if the assumed battery model is also R-int. Further, the cost of reduced order approximation is demonstrated at various operating conditions (in terms of the signal-to-noise ratio (SNR)) where the assumed model was more generic than the one assumed by the battery management system. The proposed approach is demonstrated using data collected from a cylindrical battery cell.

One of the limitations of the present work is that the proposed approach assumes that the equivalent circuit model parameters remain constant when the measurements are taken. In reality, the battery equivalent circuit model parameters are known to change with temperature, age and usage conditions, such as the state of charge of the battery. This must be addressed in future works.

Author Contributions: Conceptualization, B.B. and K.R.P.; methodology, B.B. and K.R.P.; software, P.P. and S.S.; validation, P.P. and S.S.; formal analysis, P.P.; data curation, S.S.; writing—original draft preparation, B.B., P.P. and S.S.; writing—review and editing, B.B., P.P. and S.S.; visualization, P.P. and S.S.; supervision, B.B.; project administration, B.B.; funding acquisition, B.B. All authors have read and agreed to the published version of the manuscript.

Funding: This research was funded by the Natural Sciences and Engineering Research Council of Canada (NSERC) under the Discovery Grants (DG) program [funding reference number RGPIN-2018-04557] and the Alliance program [funding reference number ALLRP 561015].

Data Availability Statement: The data presented in this study are openly available in Mendeley Data at https://data.mendeley.com/datasets/h3yfxtwkjz, accessed on 24 October 2022.

Conflicts of Interest: The authors declare no conflict of interest. The funders had no role in the design of the study; in the collection, analyses, or interpretation of data; in the writing of the manuscript; or in the decision to publish the results.

References

1. Kim, J.; Cho, B.H. State-of-charge estimation and state-of-health prediction of a Li-ion degraded battery based on an EKF combined with a per-unit system. *IEEE Trans. Veh. Technol.* **2011**, *60*, 4249–4260. [CrossRef]
2. Hentunen, A.; Lehmuspelto, T.; Suomela, J. Time domain parameter extraction method for Thévenin-equivalent circuit battery models. *IEEE Trans. Energy Convers.* **2014**, *29*, 558–566. [CrossRef]
3. Yang, J.; Xia, B.; Shang, Y.; Huang, W.; Mi, C.C. Adaptive state-of-charge estimation based on a split battery model for electric vehicle applications. *IEEE Trans. Veh. Technol.* **2017**, *66*, 10889–10898. [CrossRef]
4. Wang, X.; Wei, X.; Zhu, J.; Dai, H.; Zheng, Y.; Xu, X.; Chen, Q. A review of modeling, acquisition and application of lithium-ion battery impedance for onboard battery management. *ETransportation* **2021**, *7*, 100093. [CrossRef]
5. Balasingam, B.; Pattipati, K.R. On the Identification of Electrical Equivalent Circuit Models Based on Noisy Measurements. *IEEE Trans. Instrum. Meas.* **2021**, *70*, 1–16. [CrossRef]
6. Zhou, Z.; Cui, Y.; Kong, X.; Li, J.; Zheng, Y. A fast capacity estimation method based on open circuit voltage estimation for LiNixCoyMn1-xy battery assessing in electric vehicles. *J. Energy Storage* **2020**, *32*, 101830. [CrossRef]
7. Pan, W.; Luo, X.; Zhu, M.; Ye, J.; Gong, L.; Qu, H. A health indicator extraction and optimization for capacity estimation of Li-ion battery using incremental capacity curves. *J. Energy Storage* **2021**, *42*, 103072. [CrossRef]
8. Zheng, Y.; Cui, Y.; Han, X.; Dai, H.; Ouyang, M. Lithium-ion battery capacity estimation based on open circuit voltage identification using the iteratively reweighted least squares at different aging levels. *J. Energy Storage* **2021**, *44*, 103487. [CrossRef]
9. Ni, Z.; Yang, Y. A combined data-model method for state-of-charge estimation of lithium-ion batteries. *IEEE Trans. Instrum. Meas.* **2021**, *71*, 1–11. [CrossRef]
10. Deng, Z.; Hu, X.; Lin, X.; Xu, L.; Che, Y.; Hu, L. General discharge voltage information enabled health evaluation for lithium-ion batteries. *IEEE/ASME Trans. Mech.* **2020**, *26*, 1295–1306. [CrossRef]
11. Bian, X.; Liu, L.; Yan, J.; Zou, Z.; Zhao, R. An open circuit voltage-based model for state-of-health estimation of lithium-ion batteries: Model development and validation. *J. Power Sources* **2020**, *448*, 227401. [CrossRef]
12. Hasib, S.A.; Islam, S.; Chakrabortty, R.K.; Ryan, M.J.; Saha, D.K.; Ahamed, M.H.; Moyeen, S.I.; Das, S.K.; Ali, M.F.; Islam, M.R.; et al. A comprehensive review of available battery datasets, RUL prediction approaches and advanced battery management. *IEEE Access* **2021**, *9*, 86166–86193. [CrossRef]
13. Balasingam, B.; Ahmed, M.; Pattipati, K. Battery management systems—Challenges and some solutions. *Energies* **2020**, *13*, 2825. [CrossRef]
14. Kumar, P.; Balasingam, B.; Rankin, G.; Pattipati, K.R. Battery Thermal Model Identification And Surface Temperature Prediction. In Proceedings of the IECON 2021—47th Annual Conference of the IEEE Industrial Electronics Society, Toronto, ON, Canada, 13–16 October 2021; pp. 1–6.
15. Islam, S.; Park, S.Y.; Balasingam, B. Unification of Internal Resistance Estimation Methods for Li-Ion Batteries Using Hysteresis-Free Equivalent Circuit Models. *Batteries* **2020**, *6*, 32. [CrossRef]
16. Santoni, F.; De Angelis, A.; Moschitta, A.; Carbone, P. Analysis of the Uncertainty of EIS Battery Data Fitting to an Equivalent Circuit Model. In Proceedings of the 2021 IEEE 6th International Forum on Research and Technology for Society and Industry (RTSI), Naples, Italy, 6–9 September 2021; pp. 497–501.
17. Waag, W.; Käbitz, S.; Sauer, D.U. Experimental investigation of the lithium-ion battery impedance characteristic at various conditions and aging states and its influence on the application. *Appl. Energy* **2013**, *102*, 885–897. [CrossRef]
18. Gao, Y.; Zhang, X.; Zhu, C.; Guo, B. Global Parameter Sensitivity Analysis of Electrochemical Model for Lithium-Ion Batteries Considering Aging. *IEEE/ASME Trans. Mech.* **2021**, *26*, 1283–1294. [CrossRef]
19. Marongiu, A.; Roscher, M.; Sauer, D.U. Influence of the vehicle-to-grid strategy on the aging behavior of lithium battery electric vehicles. *Appl. Energy* **2015**, *137*, 899–912. [CrossRef]
20. Islam, S.R.; Park, S.Y.; Balasingam, B. Circuit parameters extraction algorithm for a lithium-ion battery charging system incorporated with electrochemical impedance spectroscopy. In Proceedings of the IEEE Applied Power Electronics Conference and Exposition, San Antonio, TX, USA, 4–8 March 2018; pp. 3353–3358.
21. Movahedi, H.; Tian, N.; Fang, H.; Rajamani, R. Hysteresis Compensation and Nonlinear Observer Design for State-of-Charge Estimation Using a Nonlinear Double-Capacitor Li-Ion Battery Model. *IEEE/ASME Trans. Mech.* **2021**, *27*, 594–604. [CrossRef]
22. Mondal, A.; Routray, A.; Puravankara, S. Parameter identification and co-estimation of state-of-charge of Li-ion battery in real-time on Internet-of-Things platform. *J. Energy Storage* **2022**, *51*, 104370. [CrossRef]
23. Balasingam, B.; Avvari, G.; Pattipati, B.; Pattipati, K.; Bar-Shalom, Y. A robust approach to battery fuel gauging, part I: Real time model identification. *J. Power Sources* **2014**, *272*, 1142–1153. [CrossRef]
24. Diab, Y.; Auger, F.; Schaeffer, E.; Wahbeh, M. Estimating Lithium-Ion Battery State of Charge and Parameters Using a Continuous-Discrete Extended Kalman Filter. *Energies* **2017**, *10*, 1075. [CrossRef]
25. Zhang, S.; Zhang, X. A comparative study of different online model parameters identification methods for lithium-ion battery. *Sci. China Technol. Sci.* **2021**, *64*, 2312–2327. [CrossRef]
26. Lai, X.; Wang, S.; Ma, S.; Xie, J.; Zheng, Y. Parameter sensitivity analysis and simplification of equivalent circuit model for the state of charge of lithium-ion batteries. *Electrochim. Acta* **2020**, *330*, 135239. [CrossRef]
27. Raihan, S.A.; Balasingam, B. Recursive least square estimation approach to real-time parameter identification in Li-ion batteries. In Proceedings of the IEEE Electrical Power and Energy Conference, Montreal, QC, Canada, 16–18 October 2019; pp. 1–6.

28. Rothenberger, M.J.; Docimo, D.J.; Ghanaatpishe, M.; Fathy, H.K. Genetic optimization and experimental validation of a test cycle that maximizes parameter identifiability for a Li-ion equivalent-circuit battery model. *J. Energy Storage* **2015**, *4*, 156–166. [CrossRef]
29. Bar-Shalom, Y.; Li, X.R.; Kirubarajan, T. *Estimation with Applications to Tracking and Navigation: Theory Algorithms and Software*; John Wiley & Sons: Hoboken, NJ, USA, 2004.
30. *MATLAB Version 9.12.0.1956245 (R2022a)*; The MathWorks Inc.: Natick, MA, USA, 2022.
31. Pattipati, B.; Balasingam, B.; Avvari, G.; Pattipati, K.R.; Bar-Shalom, Y. Open circuit voltage characterization of lithium-ion batteries. *J. Power Sources* **2014**, *269*, 317–333. [CrossRef]
32. Kumar, P.; Rankin, G.; Pattipati, K.R.; Balasingam, B. Model Based Approach to Long Term Prediction of Battery Surface Temperature. *IEEE J. Emerg. Sel. Top. Ind. Electron.* **2022**, 1–12. [CrossRef]